

**The spin correlation parameter and analyzing power in n-p elastic scattering at intermediate energies**

R. Abegg,<sup>(a)</sup> M. Ahmad,<sup>(b,\*)</sup> D. Bandyopadhyay,<sup>(c)</sup> J. Birchall,<sup>(c)</sup> K. Chantziantoniou,<sup>(c)</sup> C.A. Davis,<sup>(a,c)</sup> N.E. Davison,<sup>(c)</sup> P.P.J. Delheij,<sup>(a)</sup> P.W. Green,<sup>(b)</sup> L.G. Greeniaus,<sup>(a,b)</sup> D.C. Healey,<sup>(a)</sup> C. Lapointe,<sup>(b,†)</sup> W.J. McDonald,<sup>(b)</sup> C.A. Miller,<sup>(a)</sup> G.A. Moss,<sup>(b,‡)</sup> S.A. Page,<sup>(c)</sup> W.D. Ramsay,<sup>(c)</sup> N.L. Rodning,<sup>(b)</sup> G. Roy,<sup>(b)</sup> W.T.H van Oers,<sup>(c)</sup> G.D. Wait,<sup>(a)</sup> J.W. Watson,<sup>(d)</sup> and Y. Ye<sup>(b)§</sup>

<sup>(a)</sup> *TRIUMF, 4004 Wesbrook Mall, Vancouver, B.C. V6T 2A9, Canada*

<sup>(b)</sup> *Department of Physics, University of Alberta,  
Edmonton, Alberta, T6G 2N5, Canada*

<sup>(c)</sup> *Department of Physics, University of Manitoba,  
Winnipeg, Manitoba, R3T 2N2, Canada*

<sup>(d)</sup> *Department of Physics, Kent State University,  
Kent, Ohio, 44242 U.S.A.*

**Abstract**

In order to improve existing  $I=0$  phase shift solutions, the spin correlation parameter,  $A_{NN}$ , and the analyzing powers,  $A_{0N}$  and  $A_{N0}$ , have been measured in n-p elastic scattering over an angular range of  $50^\circ$ - $150^\circ$  (c.m.) at three neutron energies, 220, 325 and 425 MeV to an absolute accuracy of  $\pm 0.03$ . The data have a profound effect on various phase parameters, particularly the  $^1P_1$ ,  $^3D_2$  and  $\epsilon_1$  phase parameters which in some cases change by almost a degree. With exception of the highest energy, the data support the predictions of the latest version of the Bonn potential. Also the analyzing power data ( $A_{0N}$  and  $A_{N0}$ ) measured at 477 MeV in a different experiment over a limited angular range ( $60^\circ$ - $80^\circ$ (c.m.)) are reported here.

PACS numbers: 11.30.Er; 13.75.Cs; 13.88.+e

(submitted to Physical Review C)

## I. INTRODUCTION

The nucleon-nucleon interaction is most often described in a phase-shift parametrization<sup>1-4</sup> of the scattering matrix which explicitly conserves angular momentum, parity, time reversal and, in most cases, isospin. Various potential model calculations,<sup>5-7</sup> which are semi-phenomenological and derived from pion and heavy boson exchanges, have made significant contributions in understanding the basic nature of the nucleon-nucleon interaction, especially below the pion production threshold. Generally, a complete determination of the scattering matrix is not achieved; instead, one relies on phase-shift analyses which utilize data available over a range of angles and energies to compensate for the lack of data in some other regions of phase space. Phase-shift solutions are quite stable up to 1 GeV for the p-p system. However, in the n-p system, the  $\chi^2$  per data point for some single energy solutions<sup>1,2</sup> is significantly greater than one. This implies that the n-p data base has problems; either the systematic errors of various data points are large, or the errors as given are not properly estimated. Different phase-shift solutions also show striking disagreement in their predictions of the n-p phases. This discrepancy has been attributed to the lack of high precision data on various spin observables in n-p scattering where both the incident beam and the target are polarized.<sup>8,9</sup> The spin correlation parameter,  $A_{NN}$ , measures quite a different combination of amplitudes than the other previously measured Wolfenstein parameters. It has been shown that  $A_{NN}$  is specifically sensitive to the  $^3D_2$  and  $^1P_1$  phases and the mixing parameter  $\epsilon_1$ , as well as other partial wave phase parameters.<sup>10,11</sup> Thus a measurement of  $A_{NN}$  not only helps to reduce errors for some phases and to reduce some of the correlations among phases in the error matrix, it also helps to extract information on the isoscalar tensor part of the NN interaction.<sup>10</sup> Apart from recent IUCF data<sup>12</sup> at 181 MeV, the spin correlation parameter,  $A_{NN}$ , has not been measured between 100 and 390 MeV. There are, however,  $A_{NN}$  data available from LAMPF at 390, 465, 565 and 665 MeV.<sup>13</sup> The typical errors in the LAMPF data, obtained with a white neutron beam, are  $\pm 0.06$  to  $\pm 0.15$ ; no simultaneous measurement of left-right scattering was made. At low energy ( $\leq 50$  MeV) there are recent measurements by Klages and his group of collaborators at Karlsruhe over a wide angular range and by Schöberl *et al.* at 14 MeV and  $90^\circ$  (c.m.).<sup>14</sup> References to earlier low-energy measurements can be found in the latter. Also in 1986, Lehar *et al.* have reported measurements of  $A_{NN}$  and  $A_{N0}$  at three energies, 600, 740, and 800 MeV at SATURNE.<sup>15</sup>

This paper contains a detailed description of an experiment to measure the spin correlation parameter,  $A_{NN}$ , and analyzing powers,  $A_{0N}$  and  $A_{N0}$ , in np elastic scattering at three energies, 220, 325 and 425 MeV over an angular range of  $50^\circ$ - $150^\circ$  c.m. to an absolute accuracy of  $\pm 0.03$ . The indices in the subscripts denote the direction of beam (first index) and target (second index) polarization vector,  $\hat{N}$  being normal to the scattering plane. Very precise analyzing power data ( $A_{0N}$  and  $A_{N0}$ ) were also obtained in a charge symmetry breaking (CSB) measurement in n-p elastic scattering at 477 MeV<sup>16</sup> and are also reported here. The latter analyzing powers were measured with the incident beam and target nucleons polarized separately, but otherwise the experimental techniques were the same as in the  $A_{NN}$  experiment, which

involved scattering vertically (normal to the scattering plane) polarized neutrons from vertically polarized protons and then measuring the left-right yields for all four combinations of beam (neutron) and target (proton) polarization states. Independent calibrations of the target polarization were made before and after the actual  $A_{NN}$  data-taking runs, measuring the target polarization to an absolute accuracy of  $\pm 0.02$ .

The experimental layout is briefly described in Sec. 2, and the analysis is described in Sec. 3. The final results and the effect of the present data on different partial waves are discussed in Sec. 4 and Sec. 5, respectively. Unless otherwise stated the following discussions are relevant only to the  $A_{NN}$  experiment. The details of the CSB experiment have already been described elsewhere.<sup>16</sup>

## II. EXPERIMENTAL LAYOUT

The layout of the experiment is shown in Fig. 1. Details of the TRIUMF polarized neutron beam facility, the detection apparatus and the frozen spin target (FST) can be found in Refs. 17–20. In the following, only a summary of the most essential elements is given.

### A. Primary proton beam

During the course of the  $A_{NN}$  experiment, the polarization of the primary proton beam was continually monitored in two polarimeters. The first polarimeter<sup>21</sup> (referred to as the In-Beam Polarimeter or IBP) is a four branch polarimeter capable of measuring both transverse components (sideways and normal) of polarization of the proton beam. This polarimeter has large acceptance (2.8 msr) and contains a hydrogenous target foil located 7.21 m upstream of the liquid deuterium ( $LD_2$ ) neutron production target. It was not used in the CSB experiment. The second polarimeter<sup>22</sup> (hereafter referred to as the CSB polarimeter), located 6.32 m upstream of the  $LD_2$  target, has a much smaller acceptance (0.16 msr) and is a two branch polarimeter measuring only the normal component of polarization. The proton beam polarizations were measured by scattering the beam off a Kapton foil ( $CH_2$  foil in the IBP) and then measuring the left-right (also up-down in the case of the IBP) scattering asymmetry at  $17^\circ$ . Periodically the Kapton foil in the CSB polarimeter was replaced by  $CH_2$  and graphite foils. This was done in order to account for the possible continuous hydrogen loss, for pump oil deposition on and wrinkling in the Kapton foil, and to measure the quasi-free ( $p, 2p$ ) background from carbon. The average magnitude of the proton beam polarization as measured in the CSB polarimeter was 0.72 at 425 MeV, 0.75 at 325 MeV, and 0.80 at 220 MeV. The proton beam polarization was measured to an accuracy of  $\pm 1.5\%$ . The statistical contribution to this uncertainty is negligible, the error being dominated by the uncertainty in the polarimeter analyzing powers which were deduced from the SP88 version of Arndt's phase-shift solutions.<sup>23</sup>

The CSB polarimeter also included a beam energy monitor (BEM) assembly consisting of a stack of six 10 mm thick scintillators each separated by 1 mm Cu sheets. The average relative energy of the incident proton beam was measured by determining the relative number of stopping protons in each of the six scintillators. The integrated

beam flux was determined from a secondary electron emission monitor (SEM) located at the downstream end of the proton beam line and was checked by taking the sums of left and right counts in the polarimeters after appropriate corrections.

### B. Neutron beam production and transport

Polarized neutrons were produced via the quasi-elastic reaction  $D(\vec{p}, \vec{n})2p$  from a liquid deuterium(LD<sub>2</sub>) target, 197 mm long and 51 mm in diameter. The target walls were made of 0.25 mm thick stainless steel with 0.051 mm thick stainless steel end windows. The target was designed to operate with either liquid deuterium or liquid hydrogen. The  $A_{NN}$  experiment was done at three incident proton beam energies: 235, 343 and 445 MeV. The corresponding neutron beam energies at the 9° extraction port were:  $220 \pm 2$ ,  $325 \pm 2$ , and  $425 \pm 2$  MeV. The energies followed from kinematics, taking into account the energy loss of the incident proton beam in the LD<sub>2</sub> target and the shape of the neutron spectrum as calculated by Bugg and Wilkin.<sup>24</sup> The energy spread (FWHM) as calculated by Bugg and Wilkin,<sup>24</sup> varied from 11 MeV at 220 MeV to 15 MeV at 425 MeV. The CSB experiment was performed at  $477 \pm 2$  MeV where the spread in the neutron beam energy was calculated to be 15 MeV.

The magnitude of the sideways to sideways quasi-elastic spin transfer coefficient,  $r_t$ , reaches a maximum at about 9°(lab), the angle of the extraction port for neutrons in beam line 4A/2 at TRIUMF. In order to take advantage of the large value of  $r_t$ , the polarization direction of the primary proton beam was rotated into the horizontal plane by a spin precession solenoid (L), placed 1.5 m upstream of the LD<sub>2</sub> target. The neutrons produced in the LD<sub>2</sub> target attain a net polarization ( $P_n$ ) in the horizontal plane given by

$$P_n = \sqrt{r_t^2 + r_t'^2} P_p, \quad (1)$$

where  $P_p$  is the proton polarization as measured by the proton polarimeters and  $r_t'$  is the sideways to longitudinal spin transfer coefficient. Since the neutron production is a quasi-elastic reaction, the polarization transfer coefficients from phase-shift analyses for n-p elastic scattering have to be corrected for final-state interaction effects.<sup>24</sup> To distinguish the spin transfer coefficients, those in the quasi-elastic reaction  $D(\vec{p}, \vec{n})2p$  are denoted by  $r_t$  and  $r_t'$  whereas the spin transfer coefficients in n-p elastic scattering  $H(\vec{n}, \vec{p})n$  are denoted by  $R_t$  and  $R_t'$ .

After passing through the LD<sub>2</sub> target the primary proton beam was deflected by a dipole magnet and transported to the beam dump. The neutron beam was defined by a 3.37 m long collimator consisting of steel pipes welded to a steel, lead-filled frame with steel inserts. The aperture of the collimator varied from 39.1 mm wide by 18.6 mm high upstream to 46.1 mm wide and 32.2 mm high downstream.

The neutron beam then passed through two spin precession dipole magnets. The first dipole (V) had its magnetic field pointing up (vertical) and rotated the neutron spin to lie along the beam direction. It also had a second collimator between the pole faces which was 0.61 m long and 51.3 mm by 50.8 mm in aperture, and was made of stacked lead bricks. This collimator reduced the beam halo consisting of neutrons scattered from the walls of the first collimator. The V magnet also removed charged particles from the neutron beam. The second dipole magnet (H) had a horizontal

magnetic field pointing left (when viewed along the beam direction). It rotated the longitudinal neutron spin by  $90^\circ$  into a direction perpendicular to the scattering plane.

In order to monitor possible neutron beam position changes at the FST correlated with proton beam spin reversal, a neutron beam profile monitor was installed 4.03 m downstream of the FST. The neutron beam profile was measured by using two delay line wire chambers (DLC's) to track the charged particles back to their production point in a converter scintillator. The neutron beam profile at the FST, 12.85 m downstream of the  $LD_2$  target, was approximately 56 mm high (FWHM) and 78 mm wide (FWHM). The beam centroid was stable to within  $\pm 2$  mm.

The neutron polarimeter, located just downstream of the profile monitor, was used to measure the horizontal and vertical asymmetries, which were then compared with the values obtained from the proton polarimeter (IBP). The difference in analyzing powers arising from the different vertical and horizontal beam profiles was not significant. Since the effective analyzing power was not well known, only the relative values of the sideways and normal components of the neutron beam polarization could be inferred from these asymmetries.

### C. Frozen spin polarized proton target

A frozen spin polarized proton target<sup>20</sup> was used in the experiment. The target material consisted of 1.5 mm diameter butanol ( $C_4H_{10}O$ ) beads immersed in a bath of 94%  $^4He$  and 6%  $^3He$ . Polarization of the target took place in the 2.5 T magnetic field of a superconducting solenoid. Once the desired polarization was obtained, as determined from nuclear magnetic resonance (NMR) measurements, the target temperature was lowered to about 40 mK to "freeze" the polarization. The solenoid was lowered and a room temperature solenoid above the target cell was energized to supply, together with the superconducting solenoid, the 0.257 T holding field. The entire operation took about 6-7 h and was repeated every couple of days depending on the measurement program. The  $A_{NN}$  measurements were made for one direction of the holding field with two directions of the target polarization. The CSB experiment involved all combinations of holding field directions and target polarization states.

The maximum target polarization obtained during the experiment was about 84% with typical decay times from 100-600 h. The target cell was rectangular in shape, 20 mm thick, 35 mm wide and 50 mm high. In the CSB experiment the target cell was a 40 mm diameter and 40 mm high cylinder. The position of the target cell and the precise volume occupied by the butanol beads in the cell were determined from X-ray radiographs taken at the beginning and end of all the data-taking runs. The bead filling fraction was  $0.58 \pm 0.02$ ; the density of the bead material was 0.96 g/ml. In the  $A_{NN}$  measurement there were two orientations of the target cell. In the first phase of the experiment, which was carried out at the forward proton angles ( $20^\circ$ - $45^\circ$  lab), the target cell was oriented with its 20 mm side along the beam. For the second phase of the experiment, at backward proton angles, the target cell was rotated by  $90^\circ$ , so that the 35 mm side was parallel to the beam, in order to reduce multiple scattering of the recoil protons.

#### D. Proton detection system

Figure 2 shows the layout of the experimental detection system. The recoil protons were detected in two detector assemblies mounted on booms symmetrically placed around the incident neutron beam direction. Each boom supported a time-of-flight system for energy determination and a set of four DLC's for track reconstruction and hence measurement of the scattering angle.

The proton time-of-flight system consisted of a 0.8 mm thick start scintillator (PTOF) and a 6.4 mm thick stop scintillator (E-counter). The start scintillator was placed 0.40 m from the FST center and was viewed by phototubes at opposite ends; the timing signal for each tube as well as their hardware mean time were recorded. The E-counter was a 0.65 m by 0.67 m scintillator located 3.4 m from the target. There were four phototubes attached to this scintillator, two on each of the top and bottom ends. The time-of-flight resolution was typically 8% FWHM corresponding to approximately  $\pm 0.58$  ns for recoil protons of central energy equal to 370 MeV. There was another scintillator on each boom, a 0.67 m by 0.67 m and 6.4 mm thick  $\Delta E$  counter placed before the E-counter. In the CSB experiment a wedge degrader was placed between the  $\Delta E$  and E counters to have elastically scattered protons with approximately the same energy distribution at the E-counter; a veto counter placed at the end of each boom was used to tag energetic protons from (n,np) reactions. The DLC on each boom closest to the FST had an active area of 0.3 m by 0.3 m. The three subsequent DLC's on the boom were larger, each with an active area of 0.58 m by 0.58 m. In the CSB experiment all four chambers had active areas of 0.58 m by 0.58 m. All chambers consisted of single anode planes sandwiched between cathode foils. The spacing between the planes was kept constant by flowing the chamber gas under pressure, enough to counter-balance the electrostatic attraction between the cathode and anode planes.

#### E. Neutron detection system

Scattered neutrons were detected in two large, identical scintillator arrays placed at angles conjugate to the elastic proton scattering angles. Each array was made of two vertical banks of seven 1.05 m long, 0.15 m deep and 0.15 m high horizontal scintillator bars. In order to discriminate against charged particles, three overlapping VETO scintillators were placed in front of each array. Behind each bar of the rear bank of each neutron array there was a set of seven small 70 mm wide, 64 mm high and 7 mm thick "button" scintillators, embedded in a lucite light guide. The signals from the protons which penetrated to the button counters were used to adjust the pulse height and time delays for each scintillator bar. For the CSB experiment the button events were observed at the same time as n-p elastic scattering events and were used for calibrations every two hours of data taking. In the  $A_{NN}$  experiment the calibrations were done at the beginning of each phase of the two data-taking runs. The arrays were put at forward angles where the passing protons were sufficiently energetic to penetrate the two stacks of scintillator bars. Data taken under this condition were analyzed off line immediately. On the basis of this analysis the phototube voltages

and the different time delays in the bars were adjusted to the desired values. A 1.6 mm thick scintillator (NTOF) placed 0.5 m from the target guaranteed that the charged particles originated at the target and provided time-of-flight information on the charged particles.

The time difference from two ends of each neutron bar gave the horizontal positions of the neutrons interacting in the bars. The vertical coordinates were determined by knowing which of the seven bars was struck. The vertical resolution for a single bar hit was  $\pm 75$  mm, corresponding to half the height of each bar. The horizontal position resolution was obtained from the difference of the positions of button events in the front and back bars and was found to be 32 mm FWHM. The neutron time-of-flight was determined from the arrival time of neutrons in the scintillator bars with respect to the proton time-of-flight start counter and then correcting for the proton time-of-flight between the target center and the start counter. Angular settings for each energy were defined before the measurements using optical alignment apparatus. These settings were checked through triangulation after the measurements. Both proton booms and neutron arrays were set and labeled to within a few mm of the predefined positions.

#### F. Target polarization calibration for the $A_{NN}$ measurement

The polarization of the target was measured at the beginning and at the end of each daily cycle by the usual NMR technique that had been shown to be accurate to within 4%.<sup>25</sup> In order to know the absolute target polarizations to better than 4%, separate calibration data were taken. Details of the calibration and analysis techniques can be found elsewhere.<sup>26</sup> In brief, an unpolarized beam of 497 MeV or 512 MeV protons was scattered from liquid hydrogen (LH<sub>2</sub>) in the liquid deuterium target vessel (normally used for neutron production) or from graphite, respectively. The secondary proton beam passed through the collimator and a superconducting solenoid placed at the exit of the collimator. The unwanted normal component of polarization resulting from scattering in the LH<sub>2</sub> or graphite target was rotated into the horizontal plane by this superconducting solenoid. The magnetic field in the two dipole magnets, V and H, was set to about 10 mT as required to correct for the deflection caused by slight misalignment of the solenoid and by the cyclotron fringe magnetic field.

The incident proton beam profile at the FST was determined by using a drift chamber placed 0.65 m upstream of the target. The scattered protons from the FST were detected using two detector assemblies mounted on booms symmetrically placed at 24° to the incident beam direction. The angles were corrected for the deflection of the incident and scattered protons due to the magnetic field at the FST. The detector elements on the booms were the same as used in the measurement of the spin correlation parameter,  $A_{NN}$ . The recoil protons were detected in coincidence in two detector arms each consisting of the central veto panel of each neutron detector array and a 0.58 m × 0.58 m DLC mounted on a rail in front of the array. The neutron array-DLC combinations were placed at about 61° on both sides of the incident beam direction after correcting for the deflection angle of the recoil protons. A scintillator

with a 0.17 m by 0.17 m aperture was installed on each recoil arm 0.5 m away from the target center to define events originating in the FST. The p-p analyzing power,  $A_p$ , is very precisely known and taken from phase-shift analyses, the typical error being 1.5%. The average incident proton beam energies were 469 MeV and 501 MeV at the FST center for the  $\text{LH}_2$  and graphite scattering targets, respectively. The average analyzing power over the  $10^\circ$  full acceptance of the scattering detectors was calculated from the expression

$$\bar{A}_p = \frac{\int A_p(\theta)w(\theta)d\theta}{\int w(\theta)d\theta}, \quad (2)$$

where the weighting function  $w(\theta)$  was determined from data taken with the target unpolarized. The central p-p analyzing power values used in the calibration are,  $A_p(24^\circ, 469\text{MeV}) = 0.4092 \pm 0.0060$  and  $A_p(24^\circ, 501\text{MeV}) = 0.4204 \pm 0.0063$ . The analyzing power values were taken from Arndt *et al.*'s energy-dependent solution SP88 with errors estimated on the basis of the differences between Arndt *et al.*'s solution SP88 and their single-energy solutions C450 and C500 (of the same data) and Bystricky *et al.*'s S500 (of February, 1987) (Ref. 23). The target polarization obtained from the proton-proton scattering asymmetries is related to the value obtained from the NMR measurements by the following expression

$$P_T(\text{scatter}) = \mu P_T(\text{NMR}). \quad (3)$$

The factor  $\mu$  was found to be equal to  $0.962 \pm 0.008(\text{stat}) \pm 0.022(\text{sys}) \pm 0.014(\text{sys})$  with the  $\text{LH}_2$  target and  $0.950 \pm 0.005(\text{stat}) \pm 0.021(\text{sys}) \pm 0.013(\text{sys})$  with the graphite target.<sup>26</sup> The first systematic error is due to the error in primary beam energy, misalignment of the apparatus, background subtraction uncertainties, the presence of various extraneous beam and FST polarization components and the error in the NMR values. The latter error was estimated to be 2.0%. This is based upon the distribution of six thermal equilibrium calibrations which showed a variance of 2.0%. The error in the enhancement factor was ten times smaller and has been neglected. The second systematic error is a scale error and is due to the uncertainty in the p-p analyzing power as determined from the phase shift analyses. The weighted average for the two values of  $\mu$  is  $0.953 \pm 0.004(\text{stat}) \pm 0.020(\text{sys}) \pm 0.014(\text{sys})$ . It is to be noted that a similar relation between the target polarization obtained using n-p scattering results and the target polarization obtained using NMR measurements was extracted for the CSB experiment. The factor  $\mu$  for that experiment was found to be equal to  $0.961 \pm 0.024 \pm (0.027)$ ,<sup>25</sup> where the error in brackets is a scale error due to uncertainty in the neutron beam polarization as deduced from phase-shift analyses and the first error is mainly due to reproducibility uncertainties in the NMR measurements.

### III. DATA ANALYSIS

A detected proton required coincident signals from the proton time-of-flight start counter, the  $\Delta E$ -counter and the E-counter, whereas a detected neutron required coincident signals from the proton time-of-flight start counter and from the neutron



scintillator array with no veto counter firing. There was no on-line rejection of data. In addition to scattering events as defined by the above trigger, scaler data corresponding to various polarimeters and detectors, the status of the FST, BEM information, and neutron beam profile information were recorded concurrently.

The proton polarimeter and BEM scalers were analyzed to determine the primary proton beam polarization and relative energy. A first estimate of the neutron beam polarization was obtained by using the appropriate transfer coefficients after correction for final-state interactions.<sup>24</sup>

### A. n-p elastic scattering events

The experimentally measured quantities consisted of polar and azimuthal angles of the neutron and proton and their kinetic energies or momenta. For two-body scattering at a known energy one azimuthal angle and any one of another, different kinematical parameter determine an n-p elastic scattering event. Observation of further parameters permits rejection of (n,n<sub>p</sub>) background. In the present analysis, four kinematical constraints were formed:

- The sum of kinetic energies of the neutron and proton :  
 $TSUM = T_p + T_n$
- The opening angle difference :  $\Delta\theta = \theta_p + \theta_n - \theta_{kin}$
- The coplanarity angle :  $\Delta\phi = \phi_p + \phi_n - 180^\circ$
- The x-component of the transverse momentum sum :  
 $P_x = P_p \cos \phi_p \sin \theta_p + P_n \cos \phi_n \sin \theta_n.$

Note that  $\theta_{kin}$  is the opening angle expected from the kinematics and is a function of the neutron scattering angle. The opening angle difference should be equal to zero degrees. Since in two-body scattering the recoil and scattered particles' azimuthal angles differ by 180°, the coplanarity angle defined above should be equal to zero degrees. Similarly, because of momentum conservation, the x-component of the transverse momentum sum should also equal zero.

The n-p elastic scattering events were selected on the basis of cuts on the summed  $\chi^2$  of the above four variables

$$\chi_{sum}^2 = \sum_{i=1}^4 \chi_i^2 = \sum_{i=1}^4 \frac{(x_i - \langle x_i \rangle)^2}{\sigma_i^2}, \quad (4)$$

where  $\sigma_i$  is the measured error in the i'th variable,  $x_i$  is the measured value of any of the above four kinematic parameters and  $\langle x_i \rangle$  is the expected value for the same quantity determined from the kinematics. The final data were chosen for  $\chi_{sum}^2 \leq 10$ . In the analysis it was verified that placing cuts on the individual  $\chi^2$  with  $\chi_i^2 \leq 5$  gave completely consistent results. In addition to the  $\chi^2$  cuts there were also cuts on the target image which is reconstructed by tracing the proton tracks back to the target. The neutron was assumed to be produced in the y-z plane of the target (i.e.  $x=0$ ), with the y and z coordinates determined by the intersection of the reconstructed proton track.

## B. Background estimate

The background contribution to the data was estimated in the following manner. First, events were selected with  $\chi_{TSUM}^2 \leq 5$ ,  $\chi_{P_x}^2 \leq 5$  and  $|\Delta\phi| \leq 6^\circ$ . The distribution in the opening angle difference was plotted under these conditions; a strong elastic scattering peak is observed at  $\Delta\theta \simeq 0^\circ$  superimposed on top of a broad background. Next the same distribution was plotted for the non-coplanar events selected on the basis of:  $\chi_{TSUM}^2 \leq 5$ ,  $\chi_{P_x}^2 \leq 5$  and  $|\Delta\phi| > 6^\circ$ . These two distributions were then matched to the tails on both sides of the elastic scattering peak. The integrated background events between the limits defined by  $\chi_{TSUM}^2 \leq 5$ ,  $\chi_{P_x}^2 \leq 5$  and  $\chi_{\Delta\theta}^2 \leq 5$  cuts on the opening angle difference distributions were then calculated for both the above two conditions. The ratio of the number of events within the specified limits of the two distributions gave an estimate of the background.

Since there was no separate background run, the background analyzing power was not known. Therefore, in calculating the systematic error arising from the background contribution, its analyzing power was assumed to be equal to one, i.e., the worst possible scenario. But note that since the background nuclei in the target cell were not polarized they did not give rise to a spin correlation term. The estimated background for 325 MeV incident neutrons with the neutron detector array set at  $67^\circ$  is 3.5% of the n-p elastic scattering events. At the same angle at 425 MeV the background is estimated to be 5%. These are the worst case situations. At forward neutron angles and at lower energies the background is at most 2-3%. In the CSB experiment separate background data were taken; the estimated background is  $\leq 1\%$ . Background data show that the average analyzing power is consistent with zero in the angular range of the latter experiment.

## IV. RESULTS AND DISCUSSIONS

The left and right yields in detectors placed symmetrically around the incident beam direction for polarized beam (first index) and polarized target (second index) are given by

$$L_{\pm\pm} = NI_{\pm}\Omega_L\epsilon_L\sigma_0(1 \pm (A_{N0}P_B + A_{0N}P_T) + P_B P_T A_{NN}) \quad (5)$$

$$R_{\pm\pm} = NI_{\pm}\Omega_R\epsilon_R\sigma_0(1 \mp (A_{N0}P_B + A_{0N}P_T) + P_B P_T A_{NN}) \quad (6)$$

$$L_{\pm\mp} = NI_{\pm}\Omega_L\epsilon_L\sigma_0(1 \pm (A_{N0}P_B - A_{0N}P_T) - P_B P_T A_{NN}) \quad (7)$$

$$R_{\pm\mp} = NI_{\pm}\Omega_R\epsilon_R\sigma_0(1 \mp (A_{N0}P_B - A_{0N}P_T) - P_B P_T A_{NN}), \quad (8)$$

where  $\sigma_0$  is the unpolarized differential cross section. The quantity  $N$  is the number of target protons per unit area,  $I$  is the integrated neutron beam intensity on the target,  $\Omega$  and  $\epsilon$  are the solid angle and efficiency, respectively, and  $P_B$  and  $P_T$  are the beam and target polarizations, respectively.

Since there were two sets of detectors set at equal angles and since there were four different spin combinations, the systematic errors arising from different detector efficiencies and solid angles cancel in first order. There were six angle settings for 220 MeV, eight for 325 MeV and seven for 425 MeV, all settings being five degrees

apart. Since the detectors spanned about ten degrees in the laboratory, there was considerable overlap between two adjacent angle settings. The data in the overlap regions were combined together by taking the weighted average.

### A. Analyzing powers, $A_{N0}$ and $A_{0N}$

The analyzing powers  $A_{N0}$  and  $A_{0N}$  can be extracted from the data by combining left and right yields in a such a way that the contribution from  $A_{NN}$  drops out, with a dependence on either the target polarization or the beam polarization alone.

(a) With the target polarization

$$A_{0N} = \frac{1}{P_T} \frac{X - 1}{X + 1}, \quad (9)$$

$$X^2 = \frac{(r_{--} + r_{+-})(l_{++} + l_{+-})}{(r_{++} + r_{-+})(l_{--} + l_{+-})} \quad (10)$$

where  $l_{++}$ , etc. are the flux normalized yields. The value of the target polarization was known from the calibration experiment.

(b) With the beam polarization

$$A_{N0} = \frac{1}{P_B} \frac{R_s - 1}{R_s + 1} \quad (11)$$

$$R_s^2 = \frac{(l_{++} + l_{+-})(r_{-+} + r_{--})}{(r_{++} + r_{+-})(l_{-+} + l_{--})}. \quad (12)$$

Apart from charge symmetry breaking effects which are predicted to be small ( $< 0.01$ ),<sup>27</sup> the analyzing powers obtained with the target and beam polarizations are expected to be equal. Thus, by equating the two analyzing powers, the absolute value of the neutron beam polarization and hence also the polarization transfer coefficient  $r_i$  can be deduced. It is to be noted that the relative values of  $r_i$  as predicted by various phase shift analyses differ by as much as 8%.

The analyzing power data obtained from a combination of yields containing the beam polarization ( $A_{N0}$ ) are listed in Table I whereas the data involving the target polarization ( $A_{0N}$ ) are listed in Table II. The errors in the tables include only the errors due to counting statistics. For each analyzing power  $A_{N0}$  data point, there is in addition a systematic error, mainly due to the presence of background and a possible misalignment of the apparatus, which is estimated to be  $\leq \pm 0.022$  at 425 MeV,  $\leq \pm 0.018$  at 325 MeV and  $\leq \pm 0.015$  at 220 MeV. Figures 3-5 show plots of the analyzing powers ( $A_{N0}$ ) at the three energies. For each analyzing power  $A_{0N}$  data point the systematic error is estimated to be  $\leq \pm 0.019$  at 425 MeV,  $\leq \pm 0.015$  at 325 MeV, and  $\leq \pm 0.014$  at 220 MeV. Note that the difference in the systematic errors for the two analyzing power data sets reflects the fact that there is no asymmetry arising from the background nuclei when the FST is polarized. The scale error in  $A_{N0}$  (assuming charge symmetry) is determined by adding in quadrature the scale error in  $A_{0N}$  and the error in the normalization factor derived by equating the two analyzing powers  $A_{N0}$  and  $A_{0N}$  at each energy.

The scale errors in  $A_{N0}$  are estimated to be 3.4% at 425 MeV, 3.2% at 325 MeV, and 3.6% at 220 MeV, while the scale errors in  $A_{0N}$  are 2.4% at all energies.

The analyzing powers from the CSB measurement are presented in Table III. The values for  $A_{N0}$  were normalized using  $\sqrt{r_t^2 + r_t'^2} = 0.764 \pm 0.013$  and a proton polarimeter analyzing power at 497 MeV and 17° lab of  $0.507 \pm 0.010$ , while the values for  $A_{0N}$  were based on  $P_T = 0.772 \pm 0.036$ . The scale uncertainties are thus estimated to be  $\pm 2.6\%$  for the  $A_{N0}$  and  $\pm 4.7\%$  for  $A_{0N}$  data. Note that the calibration experiment only pertained to the set of  $A_{NN}$  measurements. The  $A_{N0}$  and  $A_{0N}$  data of the CSB experiment as presented here should not be used as a precise test of charge symmetry breaking. Presentation of the data in the present manner does not result in the careful cancellation of all the systematic errors that was necessary for the result of Ref. 16.

### B. Spin transfer coefficient, $R_t$

Since the neutron beam polarization is related to the proton beam polarization by the expression,  $P_n = \sqrt{r_t^2 + r_t'^2} P_p$ , and since the absolute value of the neutron beam polarization was derived from the calibration experiment, the correct value of the quantity  $\sqrt{r_t^2 + r_t'^2}$  can be deduced. The quantity  $r_t'$  is small compared to  $r_t$  (predicted values are: 0.011 at 228 MeV, 0.002 at 337 MeV and 0.015 at 440 MeV), and can be neglected in first approximation. For the three incident proton energies (at the center of the LD<sub>2</sub> target), the measured transfer coefficients,  $r_t$ , at  $\theta_n = 9^\circ(\text{lab})$  are summarized in Table IV. Using Bugg and Wilkin's<sup>24</sup> prescription the transfer coefficients for free n-p scattering ( $R_t$ ) at 9° (lab) are then calculated and are also included in the table. Average neutron beam polarizations were 0.72 at 220 MeV, 0.69 at 325 MeV, and 0.61 at 425 MeV.

### C. Spin Correlation Parameter, $A_{NN}$

In terms of the ratio

$$S^2 = \frac{(l_{++} + l_{--})(r_{++} + r_{--})}{(l_{+-} + l_{-+})(r_{+-} + r_{-+})} \quad (13)$$

an expression is obtained for the spin correlation parameter

$$A_{NN} = \frac{1}{P_B P_T} \frac{(S - 1)}{(S + 1)}. \quad (14)$$

Note that  $l_{++}$ , etc. are the yields normalized with respect to the integrated beam flux. The error in  $A_{NN}$  is given by,

$$\frac{\delta A_{NN}}{A_{NN}} = \sqrt{\left(\frac{\delta P_B}{P_B}\right)^2 + \left(\frac{\delta P_T}{P_T}\right)^2 + \left(\frac{2\delta S}{(S-1)}\right)^2}, \quad (15)$$

where

$$\delta S = S \sqrt{\frac{1}{l_{++} + l_{--}} + \frac{1}{r_{++} + r_{--}} + \frac{1}{l_{+-} + l_{-+}} + \frac{1}{r_{+-} + r_{-+}}}$$

The absolute values of  $P_T$  and  $P_B$  were derived from the calibration experiment as explained above. The systematic error for each  $A_{NN}$  data point, mainly due to the presence of background, a possible misalignment of the apparatus, and the presence of extraneous components of the neutron beam polarization arising from the scattering at  $9^\circ$ , is estimated to be  $\leq \pm 0.022$  at 425 MeV,  $\leq \pm 0.019$  at 325 MeV and  $\leq \pm 0.019$  at 220 MeV. Furthermore each  $A_{NN}$  data point has associated with it a scale error of 2.7% at 425 MeV, 2.6% at 325 MeV and 3.2% at 220 MeV. The  $A_{NN}$  data are listed in Table V. Figures 6–8 show plots of the  $A_{NN}$  data together with the predictions from different phase shift analyses and the potential model calculations. The IUCF  $A_{NN}$  data measured at 181 MeV are shown together with our data measured at 220 MeV. Note that the difference between these two data sets reflects the energy dependence of the spin correlation parameter. The LAMPF data<sup>13</sup> of  $A_{NN}$  measured for a 100 MeV wide bin with an average energy of 390 MeV are also shown. At 220 MeV, 325 MeV and 425 MeV the Bonn potential predictions are those from its most recent version which extends to the energy domain beyond the pion production threshold.<sup>7</sup> The Paris potential predictions obtained from SAID are valid up to 350 MeV. However, since the inelasticities in the  $I=0$  channel of the n-p system are small below 1000 MeV, the extrapolation to 425 MeV is probably justified.

## V. EFFECT ON PHASE PARAMETERS

To determine the effect of the data on the various n-p phase parameters Arndt's scattering analysis program SAID<sup>23</sup> was used. The present  $A_{NN}$  data with a typical normalization error or scale error of  $\pm 0.03$  were incorporated into the data base of the SP88 solution of SAID. As expected, at all three energies the phase parameters  $^1P_1$ ,  $^3D_2$  and  $\epsilon_1$  are affected most strongly by the present data. This version of Arndt's scattering analysis program (SP88) also includes preliminary data on  $D_i/R_i$  measured at TRIUMF by the present collaboration.<sup>28</sup> The inclusion of the  $D_i/R_i$  data had a large effect on the mixing parameter,  $\epsilon_1$ , and the  $^3S_1$ ,  $^3D_1$  and  $^3D_2$  phases. To examine the effect of the present  $A_{NN}$  data without the  $D_i/R_i$  data, the phase shifts predicted by the SM87 solution of SAID were also considered.

The mixing parameter  $\epsilon_1$  is plotted in Fig. 9. Beyond 200 MeV, the Bonn and Paris potential predictions of  $\epsilon_1$  diverge from each other. It appears that with the new TRIUMF data the mixing parameter  $\epsilon_1$  saturates around  $5^\circ$  at the higher energies; the trend is in rough agreement with the prediction of the latest version of the Bonn potential.<sup>7</sup> Note that this version of the Bonn potential predicts a lower D-state probability,  $P_D \simeq 4.9\%$ , compared to the Paris potential which predicts  $P_D \simeq 5.8\%$ . A low  $P_D$  corresponds to a weak tensor force and a more realistic value for the triton binding energy.<sup>6,7</sup> Also shown in Fig. 9 are low energy preliminary values of  $\epsilon_1$  of Klages *et al.*<sup>14</sup> The n-p data of Klages *et al.* have improved the situation for  $\epsilon_1$  at lower energies considerably, but still the remaining uncertainties are large and thus preclude the selection of one potential model over the other. Clearly further

improvement in the knowledge of the  $\epsilon_1$  mixing parameter is of great importance for better determining the isoscalar tensor interaction.

The phase parameter  ${}^3D_2$  is shown in Fig. 10. The  ${}^3D_2$  phase predicted by the Paris potential is considerably greater than the predictions from the Bonn potentials and the phase-shift analyses beyond 200 MeV. This discrepancy in the  ${}^3D_2$  phase is the most probable cause of the poor agreement of the Paris potential predictions for  $A_{NN}$  with the data. The predictions of the latest version of the Bonn potential<sup>7</sup> appear to be closest to the phase-shift analysis results.

The analyzing power data were also included separately in the program SAID. Some of the phase parameters are affected; however, the effect is not very large. This reflects the fact that the analyzing power data at 425 MeV obtained in the present experiment lie in between the earlier BASQUE<sup>30</sup> and LAMPF<sup>29</sup> data. The effect of the  $R_t$  data on various phase parameters was also investigated. It is found that at 325 MeV the  ${}^1P_1$ ,  ${}^3S_1$  and  ${}^3D_3$  phases are changed by  $0.14^\circ$ ,  $0.11^\circ$ , and  $0.10^\circ$ , respectively.

## VI. CONCLUSIONS

The spin correlation parameter  $A_{NN}$  and the analyzing powers  $A_{N0}$  and  $A_{0N}$  have been measured with absolute accuracy of  $\pm 0.03$  in n-p elastic scattering. Prior to the present experiment there were no precise  $A_{NN}$  data available over a wide range of intermediate energies. The 220 MeV  $A_{NN}$  data agree quite well with the extended Bonn potential prediction in the intermediate and backward angle range. At 325 MeV the shape of the angular distribution of  $A_{NN}$  closely resembles the extended Bonn potential prediction; however, the absolute values differ. At 425 MeV the agreement is rather poor. The spin correlation parameter  $A_{NN}$  is the more sensitive observable to be compared with potential model predictions. The longstanding problem of the differences in the measured values of the 425 MeV analyzing power data is partly resolved. Renormalization of the LAMPF  $A_{0N}$  data<sup>29</sup> by 0.890 brings the LAMPF data very close to the results of the present measurement, both in magnitude and in the shape of the angular distribution. The renormalization constant is within the allowed limits given for the LAMPF data. Because of the difference in shape it is not possible to renormalize the BASQUE 425 MeV  $A_{N0}$  data<sup>30</sup> to fit the results of the present experiment. Also, at 325 MeV, at forward angles, the BASQUE  $A_{N0}$  data show a significant deviation from the present data and also from the phase-shift predictions of Arndt. Further comments on this situation are found in the following paper.<sup>4</sup>

The present data have a great impact on the phase-shift parametrization of the  $l=0$  scattering amplitudes. The present data will definitely help refine the commonly used nucleon-nucleon potentials such as the Paris and Bonn potentials of importance for nuclear structure calculations.

This work is supported in part by the Natural Sciences and Engineering Research Council of Canada. The support of TRIUMF technical staff for a smooth running of the experiment is acknowledged.

## References

\*Present address: Department of Medical Physics, Memorial Sloan-Kettering Cancer Center, 1275 York Avenue, New York, U.S.A. 10021

†Present address: Saskatoon Cancer Clinic, Saskatoon, Saskatchewan, Canada S7K 6Z2.

‡Present address: Science World, Vancouver, British Columbia, Canada, V6B 5E7.

§Present address: Nuclear Physics Division, Department of Technical Physics, Beijing University, Beijing, China 100871.

1. R. A. Arndt, J. S. Hyslop, and L. D. Roper, *Phys. Rev. D* **35**, 128 (1987).
2. J. Bystricky, C. Lechanoine-Leluc and F. Lehar; *J. Physique* **48**, 199 (1987).
3. R. Dubois, D. Axen, R. Keeler, M. Comyn, G. A. Ludgate, J. R. Richardson, N. M. Stewart, A. S. Clough, D. V. Bugg and J. A. Edgington, *Nucl. Phys.* **A377**, 554(1982).
4. D. V. Bugg, *Phys. Rev. C*, this issue.
5. M. Lacombe, B. Loiseau, J. M. Richard, R. Vinh Mau, P. Pirès and R. de Tourreil, *Phys. Rev. D* **12**, 1495 (1975); M. Lacombe, B. Loiseau, J. M. Richard, R. Vinh Mau, J. Côté, P. Pirès and R. de Tourreil, *Phys. Rev. C* **21**, 861 (1980); R. Vinh Mau, in *Mesons in Nuclei*, ed. by M. Rho and D. H. Wilkinson (North Holland Publishing Co., Amsterdam, 1979), Vol. I, p 151.
6. R. Machleidt, K. Holinde and Ch. Elster, *Phys. Rep.* **149**, 1 (1987).
7. R. Machleidt, Private communication and also in *Adv. Nucl. Phys.* **19**, 1 (1988).
8. D. V. Bugg, J. A. Edgington, W. R. Gibson, N. Wright, N. M. Stewart, A. S. Clough, D. Axen, G. A. Ludgate, C. J. Oram, L. P. Robertson, J. R. Richardson and C. Amsler, *Phys. Rev. C* **21**, 1004 (1980).
9. W. T. H. van Oers. *Nucl. Phys.* **A463**, 517c (1987).
10. J. Binstock and R. Bryan. *Phys. Rev. D* **9**, 2528 (1974).
11. G. S. Chulick, Ch. Elster, R. Machleidt, A. Picklesimer and R. M. Thaler, *Phys. Rev. C* **37**, 1549 (1988).
12. J. Sowinski, R. C. Byrd, W. W. Jacobs, S. E. Vigdor, C. Whiddon, S. W. Wissink, L. D. Knutson and P. L. Jolivet; *Phys. Lett.* **B199**, 341 (1987).
13. T. S. Bhatia, G. G. Glass, J. C. Hiebert, L. C. Northcliffe, W. B. Tippens, B. E. Bonner, J. E. Simmons, C. L. Hollas, C. R. Newsom, R. D. Ransome and P. J. Riley in *Polarization Phenomena in Nuclear Physics - 1980*, ed by G. G. Ohlson, R. E. Brown, N. Jarmie, W. W. McNaughton and G. M. Hale, AIP Conference Proceedings, No 69, p. 123.

14. H. O. Klages, 1988, Private communication; M. Schöberl, H. Kuiper, R. Schmelzer, G. Mertens, and W. Tornow, *J.Phys* **G10**, L247 (1984).
15. F. Lehar, A. de Lesquen, L. van Rossum, P. Chaumette, J. Derégel, J. Fabre, M. de Mali, D. Legrand, F. Perrot, J. Ball, C. D. Lac, P. Bach, R. Hess, Ph. Sormani, D. Adams, J. Bystricky, V. Ghazikhanian, Contribution to the VII International Symposium on High Energy Spin Physics, Protvino (1986), Vol. II, p. 126.
16. R. Abegg, D. Bandyopadhyay, J. Birchall, E. B. Cairns, G. H. Coombes, C. A. Davis, N. E. Davison, P. P. J. Delheij, P.W.Green, L.G.Greeniaus, H.P. Gubler, D. C. Healey, C. Lapointe, W.P.Lee, W.J.McDonald, C. A. Miller, G. A. Moss, G. R. Plattner, P.R.Poffenberger, W. D. Ramsay, G. Roy, J. Soukup, J. P. Svenne, R. R. Tkachuk, W. T. H. van Oers, G. D. Wait and Y. P. Zhang, *Phys. Rev. Lett*, **56**, 2571 (1986); *Phys Rev. D* **39**, 2464 (1989).
17. D. Bandyopadhyay, Ph. D. Thesis, University of Manitoba, 1988, unpublished.
18. R. Abegg, J. Birchall, E. B. Cairns, G. H. Coombes, C. A. Davis, N. E. Davison, P.W. Green, L.G. Greeniaus, H.P. Gubler, W.P. Lee, W.J. McDonald, C. A. Miller, G. A. Moss, G. R. Plattner, P.R. Poffenbrger, G. Roy, J. Soukup, J. P. Svenne, R. R. Tkachuk, W. T. H. van Oers and Y. P. Zhang, *Nucl. Instr. and Meth.* **A234**, 11 (1985).
19. R. Abegg, J. Birchall, E. E. Cairns, G. H. Coombes, C. A. Davis, N. E. Davison, P.W. Green, L.G. Greeniaus, H.P. Gubler, W.P. Lee, W.J. McDonald, C. A. Miller, G. A. Moss, G. R. Plattner, P.R. Poffenberger, G. Roy, J. Soukup, J. P. Svenne, R. R. Tkachuk, W. T. H. van Oers and Y. P. Zhang, *Nucl. Instr. and Meth.* **A234**, 20 (1985).
20. P. P. J. Delheij, D. C. Healey and G. D. Wait, *Nucl. Instr. and Meth.* **A264**, 186 (1988).
21. R. Abegg and R. Schubank, TRIUMF report, TRI-DN-87-17, unpublished, 1987.
22. L. G. Greeniaus and J. Soukup, TRIUMF report, TRI-DN-81-1, unpublished, 1981.
23. R. A. Arndt. SAID, an interactive dial-in program for scattering analyses, solutions SM87 and SP88. The Saclay-Geneva and Basque phase shift analysis results and the Paris and Bonn I potential predictions are also obtained from SAID.
24. D. V. Bugg and C. Wilkin, *Nucl. Phys.* **A467**, 575 (1987). Also D. V. Bugg private communication.



25. R. Abegg, D. Bandyopadhyay, J. Birchall, E. B. Cairns, G. H. Coombes, C. A. Davis, N. E. Davison, P. P. J. Delheij, P.W. Green, L.G. Greeniaus, H.P. Gubler, D. C. Healey, C. Lapointe, W.P. Lee, W.J. McDonald, C. A. Miller, G. A. Moss, G. R. Plattner, P.R. Poffenberger, W. D. Ramsay, G. Roy, J. Soukup, J. P. Svenne, R. R. Tkachuk, W. T. H. van Oers, G. D. Wait and Y. P. Zhang, Nucl. Instr. and Meth., **A254**, 469 (1987).
26. K. Chantziantoniou, M. Sc. Thesis, University of Manitoba, 1989, unpublished.
27. M. J. Iqbal and J. A. Niskanen, Phys. Rev. C **38**, 2259 (1988).
28. R. Abegg., D. Bandyopadhyay, J. Birchall, C. A. Davis, N. E. Davison, P.W. Green, L.G. Greeniaus, C. Lapointe, C. A. Miller, G. A. Moss, S. A. Page, W. D. Ramsay, R. R. Tkachuk, and W. T. H. van Oers, Phys Rev. C **38**, 2173 (1988).
29. C. R. Newsom, Ph. D. Thesis, University of Texas at Austin, 1980, unpublished.
30. A. S. Clough, D. R. Gibson, D. Axen, R. Dubois, L. Felawka, R. Keeler, G. A. Ludgate, C. J. Oram, C. Anslar, D. V. Bugg, J. A. Edgington, L. P. Robertson, N. M. Stewart, J. Beveridge and J. R. Richardson, Phys. Rev. C **21**, 988 (1980).

Table 1: Analyzing Power,  $A_{N0}$ . Note that each data point at 220 MeV has a systematic uncertainty of  $\pm 0.015$  and a scale error of 3.5%, at 325 MeV of  $\pm 0.018$  and 3.1% and at 425 MeV of  $\pm 0.022$  and 3.3%.

Neutron energy 220 $\pm$ 2 MeV			Neutron energy 325 $\pm$ 2 MeV			Neutron energy 425 $\pm$ 2 MeV		
Angle (c.m.)	$A_{N0}$	Stat. error	Angle (c.m.)	$A_{N0}$	Stat. error	Angle (c.m.)	$A_{N0}$	Stat. error
70.97	0.232	0.011	61.89	0.180	0.010	52.24	0.232	0.017
76.89	0.170	0.010	67.92	0.114	0.008	57.92	0.176	0.015
82.84	0.062	0.010	72.59	0.011	0.007	63.65	0.078	0.014
90.33	-0.026	0.010	77.18	-0.054	0.009	69.05	0.008	0.024
95.35	-0.075	0.010	82.05	-0.106	0.008	74.50	-0.060	0.014
99.72	-0.104	0.008	86.82	-0.163	0.009	80.40	-0.163	0.014
104.31	-0.133	0.007	91.14	-0.186	0.010	86.36	-0.219	0.015
108.86	-0.133	0.008	95.16	-0.217	0.010	91.75	-0.240	0.013
113.49	-0.153	0.007	99.31	-0.236	0.009	96.06	-0.278	0.012
117.52	-0.161	0.007	103.86	-0.237	0.009	100.87	-0.279	0.010
121.84	-0.133	0.007	108.46	-0.251	0.008	105.20	-0.302	0.010
125.97	-0.145	0.007	113.12	-0.218	0.007	109.61	-0.286	0.011
130.11	-0.120	0.007	117.59	-0.199	0.006	113.87	-0.258	0.011
134.12	-0.117	0.008	122.36	-0.193	0.007	118.18	-0.225	0.011
139.48	-0.115	0.011	127.26	-0.165	0.006	122.77	-0.198	0.013
144.18	-0.089	0.015	131.67	-0.153	0.008	127.64	-0.184	0.013
-	-	-	135.74	-0.139	0.008	132.28	-0.181	0.015
-	-	-	141.12	-0.122	0.010	136.79	-0.148	0.017
-	-	-	145.92	-0.128	0.014	143.57	-0.118	0.020

Table 2: Analyzing Power,  $A_{0N}$ . Note that each data point at 220 MeV has a systematic uncertainty of  $\pm 0.014$ , at 325 MeV of  $\pm 0.015$  and at 425 MeV of  $\pm 0.019$ . The scale error of 2.5% is the same for all energies.

Neutron energy 220 $\pm$ 2 MeV			Neutron energy 325 $\pm$ 2 MeV			Neutron energy 425 $\pm$ 2 MeV		
Angle (c.m.)	$A_{0N}$	Stat. error	Angle (c.m.)	$A_{0N}$	Stat. error	Angle (c.m.)	$A_{0N}$	Stat. error
70.97	0.259	0.010	61.89	0.174	0.009	52.24	0.218	0.013
76.89	0.163	0.010	67.92	0.103	0.007	57.92	0.167	0.011
82.84	0.058	0.009	72.59	0.018	0.006	63.65	0.104	0.011
90.33	-0.020	0.010	77.18	-0.037	0.008	69.05	0.014	0.019
95.35	-0.085	0.009	82.05	-0.098	0.007	74.50	-0.066	0.011
99.72	-0.115	0.008	86.82	-0.156	0.008	80.40	-0.134	0.011
104.31	-0.143	0.007	91.14	-0.185	0.009	86.36	-0.208	0.012
108.86	-0.134	0.008	95.16	-0.225	0.009	91.75	-0.286	0.010
113.49	-0.151	0.007	99.31	-0.254	0.008	96.06	-0.292	0.009
117.52	-0.146	0.006	103.86	-0.243	0.008	100.87	-0.289	0.008
121.84	-0.146	0.007	108.46	-0.226	0.007	105.20	-0.293	0.008
125.97	-0.128	0.007	113.12	-0.231	0.007	109.61	-0.291	0.009
130.11	-0.112	0.007	117.59	-0.214	0.006	113.87	-0.254	0.009
134.12	-0.128	0.003	122.36	-0.195	0.006	118.18	-0.211	0.009
139.48	-0.122	0.011	127.26	-0.166	0.006	122.77	-0.216	0.010
144.18	-0.067	0.014	131.67	-0.147	0.007	127.64	-0.173	0.010
-	-	-	135.74	-0.142	0.008	132.28	-0.184	0.011
-	-	-	141.12	-0.111	0.011	136.79	-0.146	0.012
-	-	-	145.92	-0.107	0.015	143.57	-0.089	0.015

Table 3: Analyzing Powers  $A_{N0}$  and  $A_{0N}$  at 477 MeV. The scale error for the  $A_{N0}$  data is 2.6% while that for the  $A_{0N}$  data is 4.7%.

Angle (c.m.)	$A_{N0}$	Stat. error	$A_{0N}$	Stat. error
60.93	0.094	0.036	0.045	0.068
61.41	0.117	0.014	0.122	0.026
61.88	0.098	0.010	0.099	0.010
62.36	0.096	0.009	0.098	0.007
62.84	0.104	0.009	0.112	0.006
63.31	0.091	0.009	0.100	0.006
63.79	0.082	0.009	0.077	0.006
64.27	0.079	0.009	0.075	0.006
64.75	0.077	0.009	0.066	0.006
65.23	0.071	0.009	0.070	0.006
65.71	0.060	0.009	0.055	0.006
66.19	0.058	0.009	0.044	0.006
66.67	0.043	0.009	0.063	0.006
67.15	0.037	0.009	0.042	0.006
67.63	0.026	0.009	0.029	0.006
68.11	0.021	0.009	0.017	0.007
68.59	-0.001	0.009	0.028	0.007
69.08	0.032	0.009	0.017	0.007
69.56	-0.001	0.010	0.002	0.007
70.04	0.010	0.010	0.003	0.007
70.53	-0.009	0.010	-0.005	0.007
71.01	-0.020	0.010	-0.008	0.007
71.50	-0.036	0.010	-0.009	0.007
71.98	-0.024	0.010	-0.029	0.007
72.47	-0.046	0.010	-0.022	0.007
72.96	-0.038	0.010	-0.055	0.007
73.44	-0.051	0.010	-0.043	0.007
73.93	-0.068	0.010	-0.054	0.007
74.42	-0.065	0.010	-0.062	0.007
74.91	-0.064	0.010	-0.064	0.007
75.39	-0.086	0.010	-0.073	0.007
75.88	-0.083	0.010	-0.077	0.007
76.37	-0.087	0.010	-0.080	0.007
76.86	-0.085	0.011	-0.085	0.007
77.35	-0.099	0.011	-0.125	0.007
77.84	-0.100	0.011	-0.099	0.008
78.34	-0.108	0.012	-0.105	0.008
78.83	-0.145	0.016	-0.113	0.009
79.32	-0.137	0.032	-0.131	0.012
79.81	-0.011	0.109	-0.146	0.022

Table 1: Spin transfer coefficient,  $R_t$ , in free n-p scattering. Note the first error in the measured data is statistical whereas the second error is systematic.

Energy (MeV)	Angle in c.m. (deg)	$r_t$		$R_t$		
		Measured data	Deduced data	Arndt <sup>a</sup>	Saclay- Geneva <sup>b</sup>	Basque <sup>c</sup>
228	160.9	$-0.829 \pm 0.022 \pm 0.029$	$-0.790 \pm 0.021 \pm 0.028$	-0.885	-0.818	-0.839
337	160.5	$-0.833 \pm 0.016 \pm 0.026$	$-0.787 \pm 0.015 \pm 0.025$	-0.841	-0.793	-0.792
440	160.0	$-0.797 \pm 0.016 \pm 0.026$	$-0.760 \pm 0.015 \pm 0.025$	-0.837	-0.762	-0.753

<sup>(a)</sup> Ref. 23, <sup>(b)</sup> Ref. 2 and <sup>(c)</sup> Ref. 3

Table 5: Spin Correlation Parameters,  $A_{NN}$ . Note that each data point at 220 MeV has a systematic uncertainty of  $\pm 0.019$  and a scale error of 5.5%, at 325 MeV of  $\pm 0.019$  and 5.3% and at 425 MeV of  $\pm 0.022$  and 5.4%.

Neutron energy 220 $\pm$ 2 MeV			Neutron energy 325 $\pm$ 2 MeV			Neutron energy 425 $\pm$ 2 MeV		
Angle (c.m.)	$A_{NN}$	Stat. error	Angle (c.m.)	$A_{NN}$	Stat. error	Angle (c.m.)	$A_{NN}$	Stat. error
70.97	0.543	0.016	61.89	0.263	0.013	52.24	0.132	0.021
76.89	0.511	0.015	67.92	0.241	0.011	57.92	0.097	0.018
82.84	0.463	0.014	72.59	0.217	0.009	63.65	0.116	0.018
90.33	0.444	0.015	77.18	0.196	0.012	69.05	0.138	0.031
95.35	0.465	0.014	82.05	0.174	0.010	74.50	0.099	0.018
99.72	0.489	0.012	86.82	0.167	0.011	80.40	0.104	0.018
104.31	0.514	0.011	91.14	0.180	0.013	86.36	0.087	0.019
108.86	0.544	0.012	95.16	0.206	0.012	91.75	0.136	0.017
113.49	0.548	0.011	99.31	0.260	0.012	96.06	0.121	0.015
117.52	0.572	0.011	103.86	0.318	0.012	100.87	0.190	0.013
121.84	0.571	0.012	108.46	0.338	0.011	105.20	0.208	0.013
125.97	0.564	0.012	113.12	0.372	0.010	109.61	0.245	0.015
130.11	0.548	0.012	117.59	0.398	0.009	113.87	0.272	0.015
134.12	0.523	0.013	122.36	0.439	0.010	118.18	0.320	0.014
139.48	0.439	0.016	127.26	0.450	0.010	122.77	0.369	0.017
144.18	0.390	0.021	131.67	0.452	0.011	127.64	0.368	0.017
-	-	-	135.74	0.399	0.012	132.28	0.350	0.019
-	-	-	141.12	0.365	0.014	136.79	0.341	0.020
-	-	-	145.92	0.270	0.020	143.57	0.201	0.023

## Figure Captions

Fig. 1. : Experimental lay-out of neutron beam production and transport and monitoring (not to scale). The symbols L, V, and H in brackets refer to the magnetic field direction: longitudinal, vertical and horizontal respectively.

Fig. 2. : Lay-out of the experimental detection system for a typical set of scattering angles. The distance from the target center to the E counter is 3.4 m, the distance to the neutron arrays is a function of angle setting.

Fig. 3. : Analyzing powers,  $A_{N0}$ , at 220 MeV. The data of the present experiment are shown as open squares whereas the solid triangles are from a previous measurement by the BASQUE group (Ref. 30). The solid line is the energy dependent phase shift solution of Arndt (solution SM87) (Ref. 23)

Fig. 4. : Analyzing powers,  $A_{N0}$ , at 325 MeV. The symbols are as defined for the previous figure.

Fig. 5. : Analyzing powers,  $A_{N0}$ , at 425 MeV. The symbols are as defined for the previous figure with the solid circles from a previous LAMPF measurement(Ref. 29).

Fig. 6. : Spin correlation parameter,  $A_{NN}$ , at 220 MeV. The open squares are the results of the present measurement. For comparison the IUCF data measured at 181 MeV are also shown (solid triangles). The Bonn potential prediction (Bonn II) is taken from Ref. 7. C200 is the fixed energy solution whereas SM87 is the energy dependent solution of Arndt (Ref. 23). Saclay phase shift analysis and Paris potential predictions are taken from SAID

(Ref. 23). The SM87 data base does not include any of the recent TRIUMF n-p data.

Fig. 7. : Spin correlation parameter,  $A_{NN}$ , at 325 MeV. The symbols are as specified in the legend of Fig. 6.

Fig. 8. : Spin correlation parameter,  $A_{NN}$ , at 425 MeV. The solid circles are the LAMPF data (Ref. 13) measured at an average energy of 390 MeV. The other symbols are as specified in Fig. 6.

Fig. 9. : The energy dependence of the mixing parameter,  $\epsilon_1$ , as predicted by different phase shift analyses and potential models. The symbols are defined as follows: ■ : present data added to the 1988 data base of the SP88 solution of SAID, □ : the SM87 solution of SAID, ▲ preliminary results of Klages et al. (Ref. 14) after inclusion of the Karlsruhe data in the data base of the SP88 solution of SAID, ● : BASQUE phase shift analysis(Ref 3), △ : present data added to the data base of the BASQUE phase shift analysis (Ref. 4), — Paris potential (Ref. 5), - · - · - Bonn I potential(Ref. 6), and - - - Bonn II potential (Ref. 7) predictions.

Fig. 10. : The energy dependence of  $^3D_2$  phase shift. The symbols have the same definition as in the previous figure.



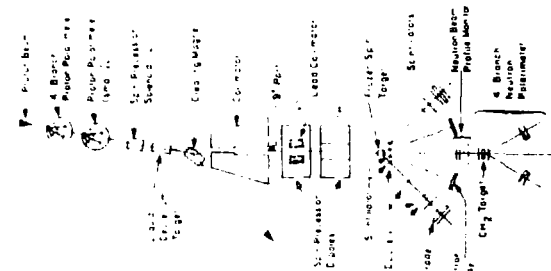


Fig. 1

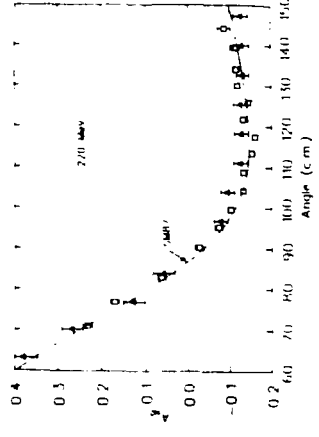


Fig. 3

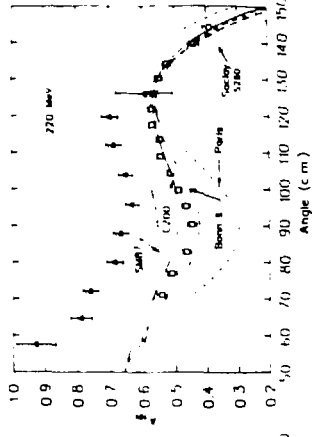


Fig. 6

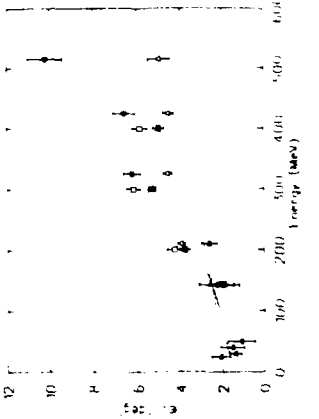


Fig. 16

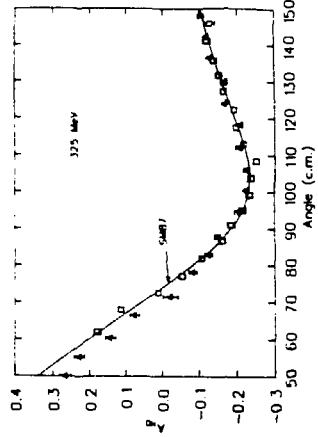


Fig. 4

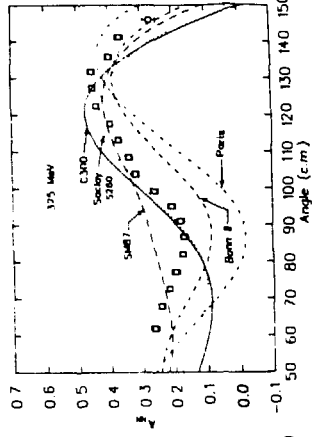


Fig. 7

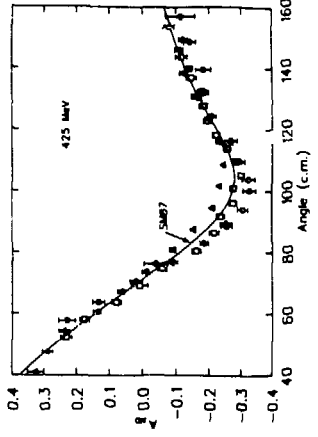


Fig. 5

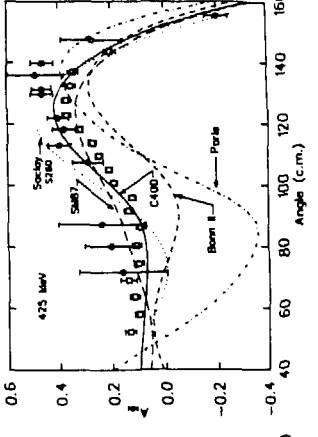


Fig. 8

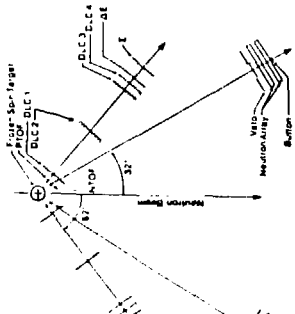


Fig. 2